J Therm Anal Calorim (2011) 106:93–99
DOI 10.1007/s10973-011-1620-8

Gelatinization and retrogradation of thermoplastic starch characterized using modulated temperature differential scanning calorimetry

Robert A. Shanks · L. M. Wasantha K. Gunaratne

NATAS2010 Conference Special Issue

Abstract Starches with varying amylose content, one hydroxypropylated high amylose starch and two thermoplastic starches (pre-gelatinized and with V type crystals) were gelatinized in the presence of added water. Gelatinization was characterized using wide-angle X-ray scattering and modulated temperature differential scanning calorimetry (mT-DSC) with a heat-cool temperature profile. The gelatinization endotherms were recorded in total heat capacity curves that were resolved into storage (reversing) and loss heat capacities, and non-reversing heat capacity curve. The endotherms were mainly of non-reversing nature, with a small contribution from the reversing component. Starch melting is a plasticizer-assisted disruption of crystals and other structures such as starch–lipid complexes and granules. Reversibility was limited since the native amylopectin crystals are rarely recrystallized and starch–lipid complexes do not reform. Recrystallization is predominantly due to subsequent slow formation of V type amylose crystals, with some B type due to recrystallization of amylopectin.

Keywords Biopolymer · Amylose · Polymorphism · Melting · Crystallization · Wide-angle X-ray scattering

Introduction

Thermoplastic starch (TPS) is a suitable environmentally friendly replacement for some conventional thermoplastics. TPS is formed by gelatinizing, or destructuring and melting, native starches in the presence of water as a plasticizer and hydrogen bond donor, a secondary plasticizer such as glycerol, and a synthetic polymer binder such as poly(oxyethylene) or poly(vinyl alcohol) may be included [1–3]. In processing starch into TPS an understanding of the structure and thermal behavior including plasticization, gelatinization, and retrogradation is crucial. Differential scanning calorimetry (DSC) and hot-stage polarized optical microscopy are methods of choice for studying starch gelatinization. The interpretation of DSC results is difficult due to various transformations occurring simultaneously during heating. Modulated temperature DSC (mT-DSC) has attracted much interest, because of its ability to distinguish apparent thermodynamic (reversing) and kinetic (non-reversing) events under the prevailing DSC modulation conditions [4]. Wide-angle X-ray scattering (WAXS) is a complementary technique to confirm supramolecular structures of starch raw materials and TPS with processing and subsequent thermal aging.

Starch is a biodegradable polysaccharide consisting of essentially linear amylose and branched amylopectin [5, 6] each consisting of α-D-glucose units, with 1,4-links and 1,6-branch connections. Starch consists of micro-scale granulates that contain crystalline regions of amylopectin and amorphous regions of amylose and amylopectin branch units. Starch has three main polymorph forms, A, B, and V. The A type is characteristic of cereal starches and the B type is found in tuber and amylose-rich starches. The A and B type crystals contain bound water molecules with the B type crystals containing a central channel where more water molecules are held. The V type is obtained when amylose crystallizes from amorphous gelatinized starch. The V type crystals can be formed where amylose is co-crystallized with compounds such as alcohols [7], iodine and fatty acids [8, 9]. The A and B types have a

R. A. Shanks (✉) · L. M. W. K. Gunaratne
CRC for Polymers, Applied Sciences, RMIT University,
GPO Box 2476, Melbourne, VIC 3000, Australia
e-mail: robert.shanks@rmit.edu.au

double helical conformation of amylopectin [10–12], whereas the V type is single stranded consisting of amylose. In the V type crystals, the co-crystallized compound occupies a channel in the center of the amylose helix. The native starch structures contain starch–lipid complexes that contribute to the supramolecular complexity within starch granules [13–17].

In this paper the gelatinization of starches with varying amylose levels and a hydroxypropylated starch are characterized using mT-DSC. Starches were scanned with added water to ensure that the gelatinization occurred within the temperature range accessible to DSC without using high-pressure sample pans, due to the need for high pan thermal conductivity when performing mT-DSC. The gelatinization endotherm is resolved into reversing and non-reversing components that are interpreted in terms of molecular processes that constitute gelatinization. X-ray data are used to characterize crystallinity of the starches.

Experimental

Raw materials: low amylose starch (waxy), high amylose starches Gelose 50 (50% amylose, A_m50), Gelose 80 (80% amylose, A_m80), and hydroxypropylated Gelose 80 (A_m80HP) were obtained from Penford Australia and used after equilibration as described in the DSC and WAXS methods. TPS were aged at 286 K and water activity, $a_w = 0.50$ for 4 and 210 days to allow formation of V type crystals.

The mT-DSC melting scans were obtained by using a heat-cool modulation from 243 to 369 K. The heat-cool program used linear segments of heating and cooling with heating rate of 6 K min^{-1} for 30 s followed by cooling at 2 K min^{-1} for 30 s, respectively. This program provided a frequency of 16.7 mHz (period = 60 s), an average heating rate of 2 K min^{-1} and temperature amplitude of 1 K. The heat flow data from the mT-DSC scans were then used to calculate the total ($C_{p,total}$), storage or reversing (C_p'), loss (C_p''), and non-reversing heat capacity ($C_{p,NR}$) curves, more correctly C_p measured under DSC conditions is the apparent heat capacity since thermodynamic equilibrium measurements cannot be obtained.

All samples for DSC were prepared using a 1:2 ratio of starch to water contents, respectively, and stored in a refrigerator for 24 h in sealed 2 atm aluminum pans before scan. This ensured an excess of water over bound water and that the gelatinization temperature range was suitably low for modulated temperature DSC conditions and the aluminum sample pans. Each sample contained about 2–5 mg starch weighed using a Mettler UMX5 microbalance. The 2 atm pressure resistant pans were preferred to other high-pressure stainless steel pans from Perkin-Elmer because the higher thermal conductivity of the aluminum pans gave better modulated temperature data. A maximum temperature of 369 K was used without mass loss. Heat-cool mT-DSC requires a baseline scan of matched empty pans scanned under the same conditions. The loss heat capacity should be zero except where a change in structure is taking place, so the C_p'' curves provide a separate control to mass retention and as to whether a scan is likely to be reliable.

Wide-angle X-ray scattering (WAXS) measurements were carried out using a Bruker AXS X-ray generator (D8 Advance model) with powder camera, using Cu Kα radiation (wave-length = 0.1542 nm) operated at 40 kV and 35 mA. The scattering angle (2θ) covered the range from 3° to 30° (θ is Bragg angle) at a step of 0.02° and sampling interval of 5 s for all materials. TPS were ground to powder under liquid nitrogen using an IKA M 20 Universal mill and conditioned at water activity, a_w of 0.50 (relative humidity, RH) and 296 K for 48 h before measurement. Data was smooth using Savitzky-Golay exponential filter that preserved features of the X-ray curves while removing noise. Crystallinity was calculated from the smoothed WAXS curves shown in Fig. 1, as the ratio of the area of the diffraction peaks to the total area under each curve using a linear baseline beneath each curve.

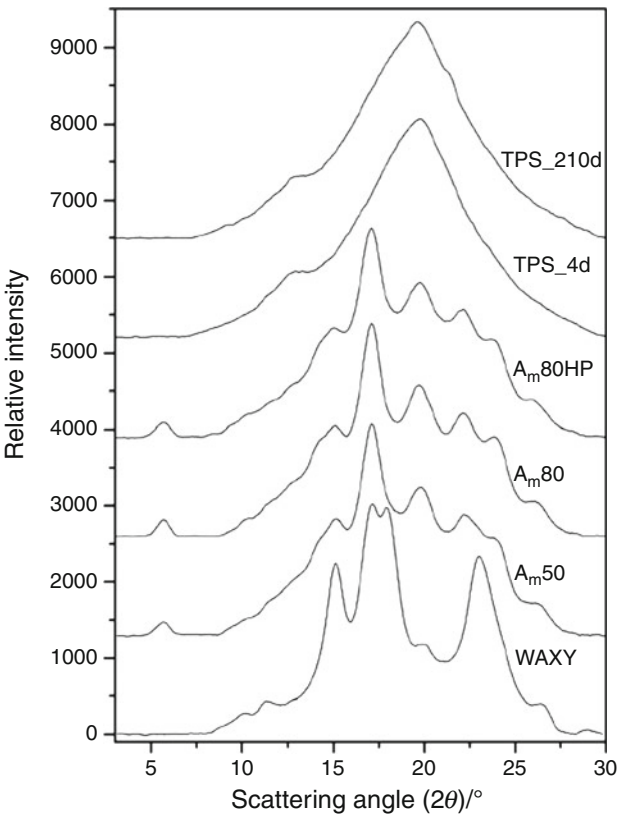

Fig. 1 WAXS of maize starch with various amylose contents and TPS (curves are offset by 1300 units)

Results and discussion

WAXS of various amylose content maize starch such as, high amylopectin (waxy), high amylose 50% (A_m50), high amylose 80% (A_m80), hydroxypropylated high amylose 80% (A_m80HP), and TPS (TPS) sheet aged for 4 and 210 days, was used to measure relative crystallinity (Fig. 1). Crystallinity was calculated as the ratio of the total area of the crystalline peaks to the total area under the X-ray curve. The waxy starch showed A type crystal structure while B type structure was observed for high amylose starches and A_m80HP. After thermoforming TPS displayed mostly gelatinized structure that is amorphous, with progressive creation of V type and B type crystal structures due to retrogradation with aging. Formation of V type crystallinity formed rapidly (4 days) and did not progress further after 210 days, as can be seen from the similarity of the two X-ray curves for TPS.

Amylose-rich maize starch dispersions amorphous part and clear reflections at 7.5°, 12.9°, 19.8°, and 22.6° (2θ), which are characteristic of the single helical crystal structure of Vh type [8]. The Vh type diffraction pattern is typical for an inclusion complex of amylose and a linear alcohol. The diffraction peaks for B type is typically at 2θ Bragg angles 5.6°, 15°, 17°, 22°, and 24° [8]. The diffraction patterns of the high amylose starches resemble that of B type starch, which is typically formed of amylose-rich maize starch. The reflections at 15° and 17° have, however, been shifted to higher 2θ values, indicating shorter distances between Bragg planes.

The relative crystallinity (Table 1) of TPS sheet was low compared with the component starches since native crystals were destroyed during extrusion and a slow recrystallization process (retrogradation) occurred afterwards. The slow retrogradation compared with unmodified high amylose starches was due to hydroxypropylation modification of starch and blending with plasticizers. High amylopectin waxy starch showed highest crystallinity that was of A type due to the crystals being of an amylopectin double helix characteristic of cereals [8, 9].

Each of the high amylose starches (regardless of amylose content, 50 or 80%) showed similar crystallinity due to B type crystals, due to the open tubular amylopectin double helix. The hydroxypropylated high amylose starch had similar crystallinity to the other high amylose starches since the hydroxypropylation reaction is performed without gelatinizing the starch.

Table 1 WAXS crystallinity of maize starch with various amylose contents and TPS

Starch	Relative crystallinity
Waxy	0.47
A_m50	0.20
A_m80	0.22
A_m80HP	0.19
TPS 210 days	0.04

The mT-DSC melting data for waxy maize starch (Fig. 2), for example, were used to calculate a total C_p curve by averaging the data over each modulation cycle. A storage C_p, or reversing C_p, curve represents the in-phase component, a loss C_p curve represents the out-of-phase component, and a non-reversing curve was calculated from the difference between the total C_p and the storage or reversing C_p data. The loss C_p represents an entropy change associated with kinetic events and it is typically zero except when there is a change in structure. Similar mT-DSC melting curves were prepared for each starch and TPS sheet. Total C_p curves for starch exhibited melting of ice (free water, T_i) at 275–276 K (not shown because of excessively high relative C_p peak) and unresolved double peaks in the starch gelatinization region and melting of amylose–lipid (T_{Am}) between 338 and 353 K. Melting of maize starch is predominately a non-reversing event with small contribution in the loss C_p curve showing that processes involved are mostly out-of-frequency ($C_{p,NR}$) or

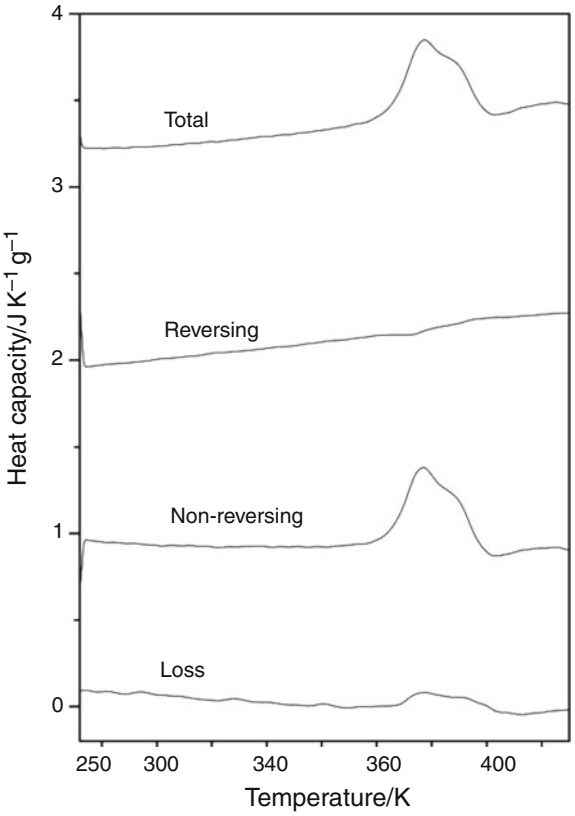

Fig. 2 mT-DSC melting curves for waxy maize starch (*Y*-axis offset for each curve)

Table 2 Thermal mT-DSC results for maize starch with various amylose contents and TPS

Starch	T_i ($C_{p,total}$)/ K	T_G ($C_{p,total}$)/ K	T_{Am} ($C_{p,total}$)/ K	T_r ($C_{p,total}$)/ K	ΔH_G ($C_{p,total}$)/ J g^{-1}	T_g (C_p')/ K	T_i ($C_{p,NR}$)/ K	ΔH_i ($C_{p,NR}$)/ J g^{-1}	T_G ($C_{p,NR}$)/ K	T_{Am} ($C_{p,NR}$)/ K	ΔH_G ($C_{p,NR}$)/ J g^{-1}	T_G (C_p'')/ K
Waxy	275.8	341.8	347.1	–	5.4	346.2	275.8	163.7	341.8	347.4	5.9	342.3
A_m50	275.1	346.3	352.5	–	3.8	–	275.0	79.4	346.3	352.5	3.9	–
A_m80	275.8	349.9	356.1	–	1.1	–	275.8	117.3	349.9	355.6	1.0	–
A_m80HP	275.6	343.1	356.1	–	1.9	–	275.7	182.6	345.9	356.2	1.9	–
TPS	274.4	337.6	–	324.2	1.1	–	273.9	108.4	337.8	–	0.6	–

in-frequency, but out-of-phase (C_p''). Ice crystals are only formed from free water in the starches so enthalpy of ice melting (ΔH_i) is less than the total water (Table 2). The remaining bound water is hydrogen bonded within the starch structure, particularly within the starch crystals.

The gelatinization, including melting of amylose–lipid complexes and their heat of fusion varied with amylose content of the starches. Treated starches exhibited higher gelatinization temperatures (T_G), improved dispersibility in hot water, less granule swelling, less shear in the gelled state and less setback [18, 19]. TPS showed broader and unresolved gelatinization and retrogradation peaks compared with the raw starches as the sheets were already gelatinized during extrusion. The inflection between 333 and 353 K in reversing C_p curves is due to a change in heat capacity due to plasticization, granule disruption, and melting of crystals. The lower temperature peak is associated with melting of amylopectin-based crystals while the higher temperature peak is associated with dissociation of amylose–lipid complexes.

Figures 3, 4, 5, and 6 show mT-DSC melting curves of starch raw materials and TPS sheets and Table 2 displays relevant thermal data. The total C_p curves of starch (Fig. 3) exhibited melting of ice (T_i) at about 275–276 K (not shown) and showed unresolved double peaks due to gelatinisation of starch (T_G) and melting of amylose–lipid complex (T_{Am}) between 338 and 353 K. The gelatinisation temperature, dissociation of amylose–lipid complexes and their heat of fusion varied with amylose content of starch. In general, treated starches exhibit higher gelatinization temperatures, improved dispersibility in hot water, less granule swelling, less shear in the gelled state and less setback [4]. The TPS showed broader and poor unresolved gelatinisation peaks and peaks due to retogradation crystal melting compared with starch as sheets that were already gelatinised during extrusion.

The total C_p curves for each starch are shown in Fig. 3. The total C_p curves show the transitions, as they would occur in a standard continuous temperature ramp DSC curve. The waxy starch exhibits the largest gelatinization endotherm and two overlapped peaks are present. The

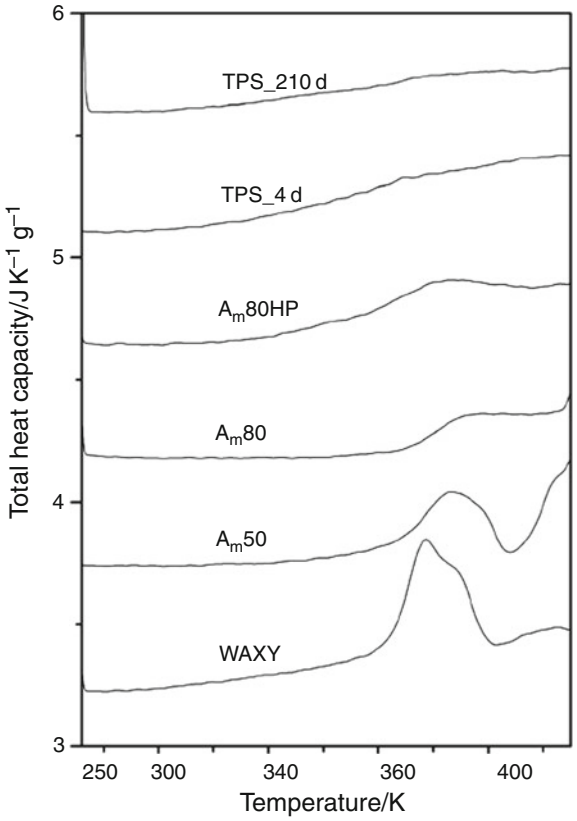

Fig. 3 Total C_p curves for each starch calculated as an average over each modulation cycle (*Y*-axis offset for each curve)

lower temperature peak corresponds to the water assisted melting of amylopectin crystals, while the higher temperature peak corresponds to the dissociation of amylose–lipid complex. The endotherms for the high amylose starches in Fig. 3 are smaller due to the overall lower crystallinity of these materials and a single broad endotherm is produced without resolving the two contributions shown by the waxy starch. The TPS materials exhibit a broad low endotherm due to the low level of V type crystallinity that has formed upon aging of the TPS for the times shown.

The reversing C_p components (Fig. 4) exhibited two transitions, one around 273 K (not shown) due to melting of ice from free water, and another transition between 333

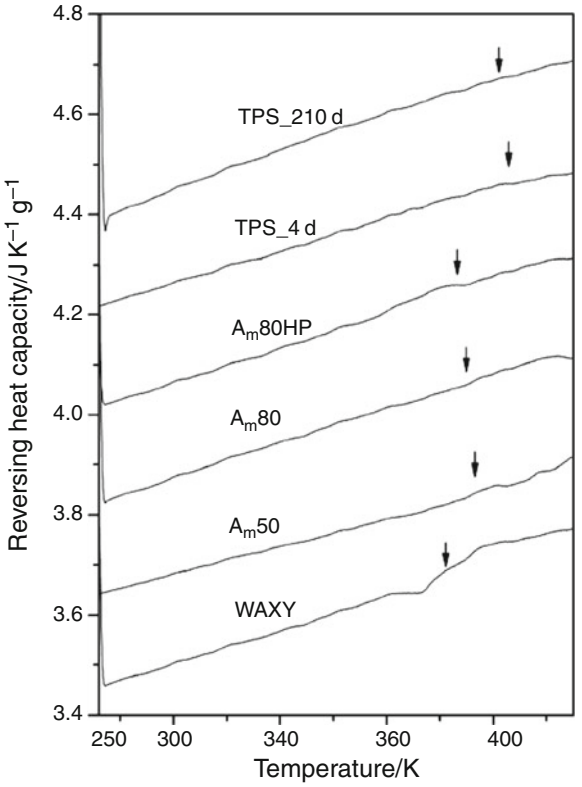

Fig. 4 Storage or reversing C_p curves for each starch (*Y*-axis offset for each curve)

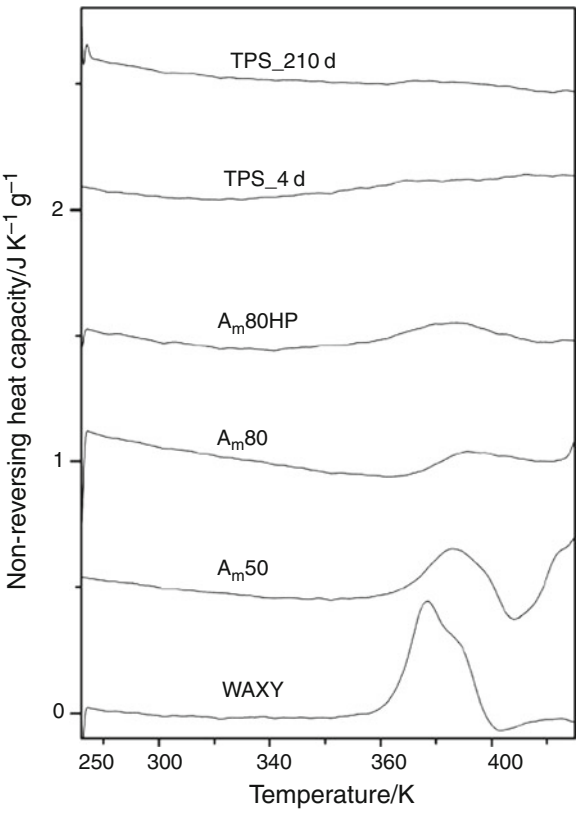

Fig. 5 Non-reversing C_p curves for each starch (*Y*-axis offset for each curve)

and 353 K. The second inflection is similar to a glass transition except for A_m80HP and TPS. Some researchers concluded this to be a glass transition [5]. However, TPS sheets and A_m80HP showed this inflection opposite (higher C_p to lower C_p) to the transition shown in the curves. This transition temperature close to melting (gelatinization) temperature is likely not a glass transition. A three-phase starch structure has been proposed [20] with a mobile amorphous phase with a sub-zero glass transition temperature, between 266 and 273 K, a rigid amorphous phase with a T_g onset of 324 K, and a crystalline phase with a melting onset of 335 K. The T_g of the mobile and rigid amorphous phases was made more apparent by annealing at a temperature of about 10 K below the expected T_g. The difference between T_g and T_m reported [20] is consistent with values expected for typical polymers where T_g and T_m are not observed to occur in the same temperature region.

An investigation using dynamic DSC (DDSC, analogous to mT-DSC) showed a stepwise inflection in the storage C_p curve that appeared like a glass transition inflection. The inflection was much decreased after removal of the amorphous phase by acid treatment. In conjunction with experiments using enzyme debranching of the starch, the authors concluded that the stepwise transition was due to a rigid amorphous phase, and that a small transition due to T_g of a mobile amorphous phase occurred just below 273 K [21].

The arrows in Fig. 4 indicate the position of the onset of the gelatinization region. Waxy starch with A type crystals shows the lowest transition temperature, followed by the three high amylose starches that exhibit B type crystals. The two TPS materials show a week C_p change, though with the highest transition temperature due to V type retrogradation crystals. The weak endotherms exhibited in the reversing heat capacity curves demonstrate that both the V and B type starch crystals only melt reversibly to a small extent, though over a long time, outside the scale of the modulated temperatures, the crystals do form again in the retrogradation process. In synthetic polymers the reversing heat capacity curves typically display melting of poorly formed crystals that can readily melt and then crystallize again, before finally melting closer to the normal melting temperature. WAXS shows that the starch crystals have diffuse structure, however, these crystal structures cannot progress markedly toward more equilibrium crystals during the modulated temperature time-scale.

The gelatinization amylopectin crystal melting and dissociation of amylose–lipid peaks can be seen in all $C_{p,NR}$ curves (Fig. 5) between 338 and 353 K for all starches. The reversing heat capacity contains the rapidly reversible

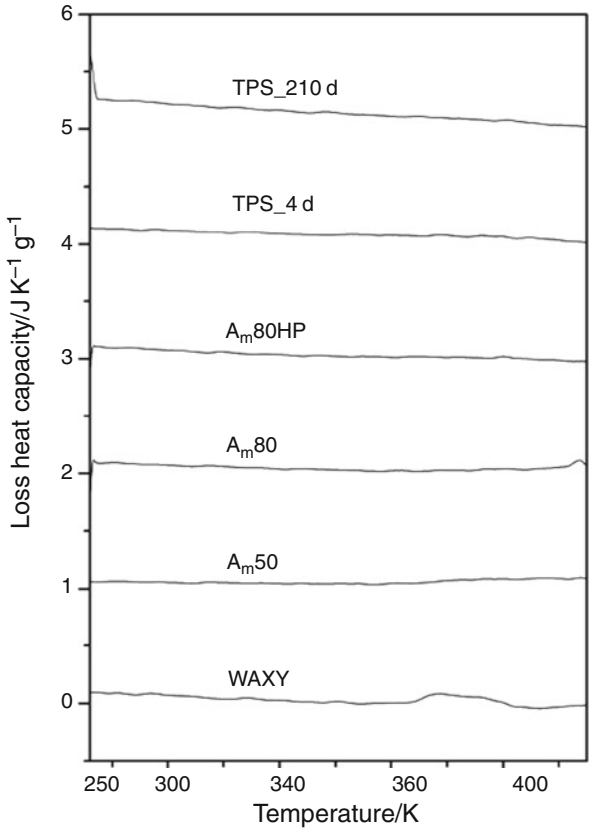

Fig. 6 Loss C_p curves for each starch (*Y*-axis offset for each curve)

component of the total heat capacity, while the non-reversing heat capacity represents the irreversible component of the total heat capacity under the particular modulation condition. The transition temperature values for each of the starches are summarized in Table 2. The melting of starch crystals is revealed to be mainly non-reversing. The non-reversing curves are almost the same as the total heat capacity curves. The melting is mostly characterized by a normal continuous scanning DSC experiment, though the modulations are expected to enhance the DSC signal due to the relatively high instantaneous heating rate (6 K min^{-1}) relative to the average heating rate (2 K min^{-1}).

The loss C_p (C_p'') curves (Fig. 6) show little detail compared with the $C_{p,NR}$ curves (Fig. 5). The C_p'' curve is normally zero except where there is a change in structure. Such a change is revealed in the curve for the waxy starch. The C_p'' is the out-of-phase component of the complex heat capacity (C_p*) and it represents a kinetic contribution, but it is different from $C_{p,NR}$ that represents all of the total C_p that is not in-phase and in-frequency. C_p'' must be contained within $C_{p,NR}$, but is does not correspond to the component that includes the endotherms for the gelatinisation transitions.

The endothermic gelatinization enthalpy represents the amount of thermal energy involved during gelatinization. Therefore, gelatinization could be the results of processes of migration of water (plasticizer) into starch granules (increasing with temperature), molecules gain thermal motions as temperature increases, cleavage of existing starch–starch –OH bonds (endothermic), formation of starch–solvent –OH bonds (exothermic) and the unwinding helix-coil transition of amylopectin helices (endothermic). The thermal processing of starch materials has been reviewed and the multiple physical reactions that occur during processing, such as water diffusion, granular expansion, gelatinization, decomposition, melting, and crystallization have been identified and discussed [22].

Conclusions

The relative crystallinity of raw starch decreased with increasing amylose content. Retrogradation crystallization produced V due to amylose and B due to amylopectin, type crystals. However, crystallinity of TPS sheets was low compared with starch, as native crystals were destroyed during extrusion and little recrystallization processes occurred afterwards. This was due to hydroxypropyl modification of starch and blending with other additives during processing. Melting endotherms were predominantly displayed in total and non-reversing heat capacity curves. The inflection between 333 and 353 K on reversing C_p curves and an endotherm in non-reversing C_p curves is with respect to changes in heat capacity due to water plasticization, granule disruption, melting and amylose–lipid complex dissociation. The loss heat capacity, out-of-phase component, reveals kinetic events related to entropy and it is different to the non-reversing heat capacity that contains out-of-frequency contributions. The starch crystal melting endotherms were mainly revealed as out-of-frequency events that they were small in the storage and loss heat capacities.

References

1. Dos Santos Rosa D, Bardi MAG, Machado LDB, Dias DB, Silva LGA, Kodama Y. Influence of thermoplastic starch plasticized with biodiesel glycerol on thermal properties of PP blends. J Therm Anal Calorim. 2010;99:675–9.
2. Schlemmer D, Sales MJA. Thermoplastic starch films with vegetable oils of Brazilian Cerrado thermal characterization. J Therm Anal Calorim. 2009;93:599–604.
3. Rudnik E. Thermal properties of biocomposites. J Therm Anal Calorim. 2009;88:495–8.
4. Gill PS, Sauerbrunn SR, Reading M. Modulated differential scanning calorimetry. J Therm Anal Calorim. 1993;40:931–9.
5. Zobel HF. Starch crystal transformations and their industrial importance. Starch. 1988;40:1–7.

6. Cura JA, Jansson PE, Krisman CR. Amylose is not strictly linear. Starch. 1995;47:207–9.
7. Manners DJ. Recent developments in our understanding of amylopectin structure. Carbohydr Polym. 1989;11:87–112.
8. Le Bail P, Bizot H, Pontoire B, Buleon A. Polymorphic transitions of amylose–ethanol crystalline complexes induced by moisture exchanges. Starch. 1995;47:229–32.
9. Le Bail P, Bizot H, Buleon A. 'B' to 'A' type phase transition in short amylose chains. Carbohydr Polym. 1993;21:99–104.
10. Godet MC, Buleon A, Tran V, Colonna P. Structural features of fatty acid–amylose complexes. Carbohydr Polym. 1993;21:91–5.
11. Wu HC, Sarko A. The double-helical molecular structure of crystalline b-amylose. Carbohydr Res. 1978;61:7–25.
12. Imberty A, Chanzy H, Pe'rez S, Buleon A, Tran V. The double-helical nature of the crystalline part of A-starch. J Mol Biol. 1988;201:365–78.
13. Imberty A, Perez S. A revisit to the three-dimensional structure of B-type starch. Biopolymers. 1988;27:1205–21.
14. Imberty A, Buléon A, Tran V, Pérez S. Recent advances in knowledge of starch structure. Starch. 1991;43:375–84.
15. Cheetham NWH, Tao L. Variation in crystalline type with amylose content in maize starch granules: an X-ray powder diffraction study. Carbohydr Polym. 1998;36:277–84.
16. Perry PA, Donald AM. The role of plasticization in starch granule assembly. Biomacromolecules. 2000;1:424–32.
17. Mani R, Bhattacharya M. Properties of injection moulded blends of starch and modified biodegradable polyesters. Eur Polym J. 2001;37:515–26.
18. Ma XF, Yu JG. Formamide as the plasticizer for thermoplastic starch. J Appl Polym Sci. 2004;93:1769–73.
19. Pavlovic S, Brandao PRG. Adsorption of starch, amylose, amylopectin and glucose monomer and their effect on the flotation of hematite and quartz. Minerals Eng. 2003;16:1117–22.
20. Sang Y, Alavi S, Shi YC. Subzero glass transition of waxy maize starch studied by differential scanning calorimetry. Starch. 2009;61:687–95.
21. Liu Y, Shi YC. Phase and state transitions in granular starches studied by dynamic differential scanning calorimetry. Starch. 2006;58:433–42.
22. Liu H, Xie F, Yu L, Chen L, Li L. Thermal processing of starch-based polymers. Prog Polym Sci. 2009;34:1348–68.